# Attitude estimation for Intervention-AUVs working in Tandem with Autonomous Surface Craft

M. Morgado[†], P. Batista[†], P. Oliveira[†] and C. Silvestre[†‡*]

[†]Institute for Systems and Robotics, Instituto Superior Técnico,
Universidade Técnica de Lisboa
Av. Rovisco Pais, 1, 1049-001, Lisbon, Portugal

[‡]Faculty of Science and Technology, University of Macau, Taipa, Macau

**Abstract**

This paper presents the design, analysis, and performance evaluation of an attitude filter for an Intervention-Autonomous Underwater Vehicle (I-AUV) working in tandem with an Autonomous Surface Craft (ASC). In the proposed framework, an ASC aids an I-AUV to determine its attitude by providing an inertial reference direction vector through acoustic modem communications, which is measured in body-fixed coordinates by an Ultra-Short Baseline (USBL) device. The specificity of the intervention mission to be carried out, near structures that distort the Earth magnetic field, renders on-board magnetometers unusable for attitude determination. The solution presented herein includes the estimation of rate gyros biases, yielding globally asymptotically stable error dynamics under some mild restrictions on the vehicle team configurations. The feasibility and performance of the proposed architecture is assessed resorting to numerical Monte-Carlo simulations with realistic sensor noise, and transmission delays and limited bandwidth of the acoustic modems.

**Keywords:** Underwater navigation, attitude estimation, Kalman filter, cooperative navigation.

## 1 Introduction

Enabling Autonomous Underwater Vehicles (AUVs) with the capability of performing precision-demanding underwater interventions involves the design and implementation of several key operational systems. Among other components, such as agile robotic actuators, thrusters, buoyancy control systems, etc., the design of precise navigation

*Email: {marcomorgado,pbatista,pjcro,cjs}@isr.ist.utl.pt

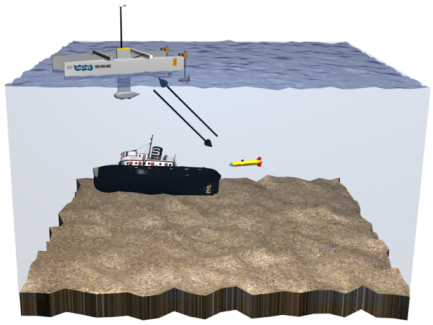

Figure 1: Vehicles during intervention phase - magnetometer is unavailable due to strong distortion by the intervention target

systems and sensor packages stands out as one of the most fundamental aspects [14]. This paper presents a novel sensor-based approach to the design of globally asymptotically stable (GAS) attitude filters with application to a team of two autonomous vehicles commissioned on a typical survey and intervention task.

Intervention-AUVs (I-AUVs) [12] are a new class of autonomous robotic vehicles that are capable of going beyond typical survey-only tasks and successfully interact with underwater subjects to perform, for instance, collection of sediment samples, deep-water oil well repairs, deactivation of underwater mines, etc. without human interaction. When operating in open water scenarios, the attitude of the vehicle is typically estimated from the fusion of information from several sensors such as accelerometers, rate gyros, Doppler Velocity Loggers (DVL), acoustic positioning systems, and from flux-gate magnetometers or digital compasses. An interesting survey on the topic of underwater vehicles navigation can be found in [17]. Typical targets, such as large metal structures, ship wrecks, metallic drills, and other Man-made objects, are known for having strong magnetic signatures which cause space anomalies and magnetic distortions [32], thus rendering the on-board magnetometers unsuitable for heading determination, but largely adopted for the detection of buried objects [18] and underwater structures investigation [24, 16].

This paper addresses the design of an AUV attitude determination system that relies upon a team of two vehicles, comprising of an Autonomous Surface Craft (ASC) and an AUV in a tandem configuration, which cooperatively navigate the surroundings of a subject of interest. The proposed framework, depicted in Fig. 1, falls within the scope of the European project TRIDENT [25] in which both vehicles are able to exchange information through acoustic modem communications and, among other sensor packages, are also suited with Ultra-Short Baseline (USBL) acoustic positioning devices and acoustic pingers / transponders. The USBL is composed of a small calibrated array of acoustic receivers that measures very accurately the Direction-of-Arrival (DOA) of the acoustic waves, given the proximity of the sensors in the receiving array.

Conventional attitude estimation algorithms are typically derived on a particular representation, e.g. rotation matrix, quaternions, Euler angles, Euler angle-axis, etc.,

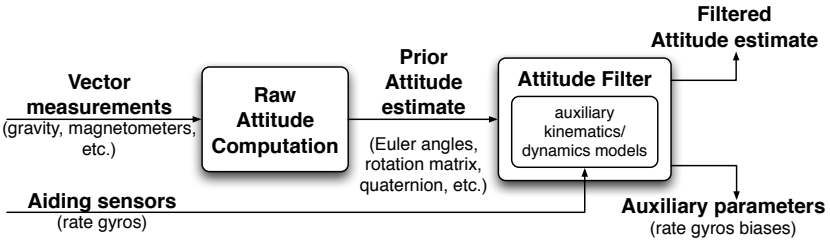


Figure 2: Classical filtering structure

see [11] for a recent thorough survey. The kinematic models, which are exact and resort to the integration of the angular velocity from three-axial rate gyros, are employed on the chosen attitude representation. These angular velocity sensors are however affected by unknown slowly time-varying biases. The adopted framework in the classical strategies is illustrated in Fig. 2, and naturally enforces the derived solutions to inherit the chosen attitude representation drawbacks, such as singularities, unwinding phenomena and/or topological limitations to achieve global asymptotic stabilization, see [7] and [10].

Solutions based on the Extended Kalman Filter (EKF) have been widely adopted in the literature, see [2] and [28] for instance. Traditional attitude filtering solutions typically convert first the available sensor vector information to an attitude representation and then filter the noisy attitude measurements. It is also well known that due to linearization of the nonlinear dynamics and observations models, EKF-like solutions are not able to achieve GAS properties. In order to tackle convergence issues, new trends have been recently adopted by the scientific community, with the design of nonlinear observers [20].

The solution proposed herein makes use of the framework presented in [3] and [6], directly including the USBL direction vector measurements in the system dynamics, while the exact kinematics are propagated using the angular velocity provided by the three-axis rate gyro. The derived solution, illustrated in Fig. 3, includes the estimation of the rate gyros biases, and yields GAS error dynamics. Adopting a Lyapunov state transformation, that preserves observability properties of the original system and allows for the nonlinear dynamics to be regarded as Linear Time-Varying (LTV), the overall system is shown to be uniformly completely observable, under some mild restrictions on the relative positions of the work team vehicles. A Kalman filter design with GAS error dynamics follows from the obtained observability results, and an optimal attitude determination algorithm is applied to the filtered vector estimates to yield the final attitude estimate.

The paper is organized as follows: Section 2 sets the problem framework and definitions. The proposed filter design and main contributions of the paper are presented in Section 3, where the filter structure is brought to full detail, and an extensive observability analysis is carried out. Simulation results and performance evaluations are discussed in Section 4, and finally Section 5 provides some concluding remarks and

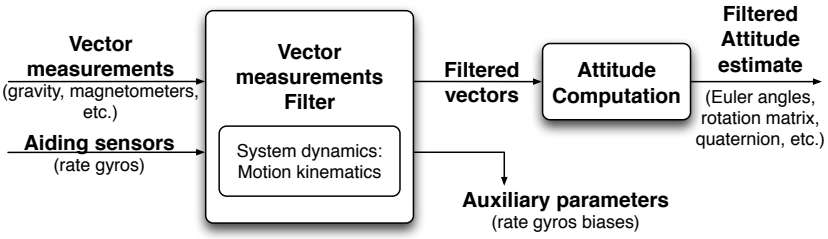


Figure 3: Proposed filtering structure

comments on future work.

### 1.1 Notation

This paper adopts the following notation: a block matrix of zeros with $n$ rows and $m$ columns is represented by the symbol $\mathbf{0}_{n\times m}$. Similarly a block of ones is represented by $\mathbf{1}_{n\times m}$, and the identity matrix with dimension $n$ is represented by the symbol $\mathbf{I}_n$. When the subscripts $n$ or $n \times m$ are omitted, the corresponding variable is of appropriate implicit dimensions. A block diagonal matrix is represented as $\mathrm{diag}(\mathbf{A_1}, \ldots, \mathbf{A_n})$. The cross product between two vectors $\mathbf{a} \in \mathbb{R}^3$ and $\mathbf{y} \in \mathbb{R}^3$ is denoted by $\mathbf{a} \times \mathbf{y}$. The operator $\|\cdot\|$ represents the typical Euclidean norm, and the set of rotation matrices is represented by the special orthogonal group $SO(3) = \left\{\mathcal{R} \in \mathbb{R}^{3\times 3} : \mathcal{R}^T\mathcal{R} = \mathcal{R}\mathcal{R}^T = \mathbf{I}_3,\ \det(\mathcal{R}) = 1\right\}$, where $\det(\cdot)$ represents the argument matrix determinant. The set of three-dimensional vectors with unit norm is denoted by $S(2) = \left\{\mathbf{x} \in \mathbb{R}^3 :\ \|\mathbf{x}\| = 1\right\}$.

## 2 Problem framework

In order to set the problem framework, let $\{I\}$ denote a local inertial frame, $\{B_{ASC}\}$ the coordinate frame attached to the body of the ASC, and $\{B_{AUV}\}$ the coordinate frame attached to the body of the AUV. The relative positions of both body frames are given by

$$\text{ASC } (s) : {}^{B_{ASC}}\mathbf{r}_u(t) = \mathcal{R}_s^T(t)(\mathbf{p}_u(t) - \mathbf{p}_s(t)), \tag{1}$$

$$\text{AUV } (u) : {}^{B_{AUV}}\mathbf{r}_s(t) = \mathcal{R}_u^T(t)(\mathbf{p}_s(t) - \mathbf{p}_u(t)), \tag{2}$$

where ${}^{B_{ASC}}\mathbf{r}_u(t) \in \mathbb{R}^3$ represents the position of the AUV relative to the ASC, expressed in the ASC body-fixed frame, ${}^{B_{AUV}}\mathbf{r}_s(t) \in \mathbb{R}^3$ is the position of the ASC represented in the AUV body-fixed reference frame, $\mathcal{R}_s(t) \in SO(3)$ and $\mathcal{R}_u(t) \in SO(3)$ are the rotation matrices that represent the attitude of the ASC and the AUV body-fixed reference frames respectively, with respect to the inertial frame $\{I\}$, $\mathbf{p}_u(t) \in \mathbb{R}^3$ and $\mathbf{p}_s(t) \in \mathbb{R}^3$ are the positions in inertial coordinates of the origins of the body-fixed reference frames of the AUV and the ASC, respectively, and the operator $(\cdot)^T$ denotes

the usual matrix transpose operation. The time-derivative of the rotation matrix $\mathcal{R}_u(t)$ verifies

$$\dot{\mathcal{R}}_u(t) = \mathcal{R}_u(t)\mathcal{S}\left[\boldsymbol{\omega}(t)\right], \tag{3}$$

where $\boldsymbol{\omega}(t) \in \mathbb{R}^3$ is the angular velocity of $\{B_{AUV}\}$ with respect to $\{I\}$, expressed in the AUV body-fixed coordinates, and $\mathcal{S}\left[\boldsymbol{\omega}(t)\right]$ is the skew-symmetric matrix that represents the cross product, such that $\mathcal{S}\left[\boldsymbol{\omega}\right] a = \boldsymbol{\omega} \times a$ and verifies $\left(\mathcal{S}\left[\boldsymbol{\omega}\right]\right)^T = -\mathcal{S}\left[\boldsymbol{\omega}\right]$. Further assume that the angular velocity readings provided by the rate gyros that are installed on the AUV are corrupted by biases $\mathbf{b}_{\boldsymbol{\omega}} \in \mathbb{R}^3$

$$\boldsymbol{\omega}_m(t) = \boldsymbol{\omega}(t) + \mathbf{b}_{\boldsymbol{\omega}}(t), \tag{4}$$

that are assumed to be constant, that is,

$$\dot{\mathbf{b}_{\boldsymbol{\omega}}}(t) = \mathbf{0},$$

or can be considered slowly time-varying if modelled as a random walk $\dot{\mathbf{b}_{\boldsymbol{\omega}}}(t) = \boldsymbol{\eta}_{\boldsymbol{\omega}}$, where $\boldsymbol{\eta}_{\boldsymbol{\omega}}$ is white Gaussian noise.

## 2.1 USBL direction vector observation

In order to extract attitude information from the on-board sensors, the first vector observation is provided by the USBL as a DOA vector measurement of the acoustic waves emitted by the ASC. The USBL computes this DOA from the Time-Difference-Of-Arrival (TDOA) of the acoustic waves arriving at the hydrophones, specially placed at known locations on the receiving array [30]. As opposed to typical acoustic relative positioning systems [30], for attitude estimation purposes the USBL can be considered to provide measurements of the DOA at a higher rate. Either from bypassing the regular interrogation-reply scheme or transmitting a known specially coded signal at a higher rate, the system can increase the update rate of the USBL direction measurements. Previous work by the authors focused on the development of a USBL with pseudo-noise coded spread-spectrum signals can be found in [23].

Denoting the position of the ASC in the AUV coordinates simply by $\mathbf{r}_s(t) := {}^{B_{AUV}}\mathbf{r}_s(t)$, and differentiating (2) in time yields

$$\dot{\mathbf{r}}_s(t) = -\mathcal{S}\left[\boldsymbol{\omega}(t)\right]\mathbf{r}_s(t) + \mathbf{v}_{\mathbf{r}}(t), \tag{5}$$

where $\mathbf{v}_{\mathbf{r}}(t) \in \mathbb{R}^3$ is the relative velocity between both vehicles, given by

$$\mathbf{v}_{\mathbf{r}}(t) = \mathcal{R}_u^T(t)\,{}^I\mathbf{v}_s(t) - \mathbf{v}_u(t), \tag{6}$$

where $\mathbf{v}_u(t) \in \mathbb{R}^3$ is the AUV velocity expressed in the AUV body-fixed reference frame, and ${}^I\mathbf{v}_s(t) \in \mathbb{R}^3$ is the ASC velocity expressed in inertial coordinates, which satisfies ${}^I\dot{\mathbf{p}}_s(t) = {}^I\mathbf{v}_s(t)$.

The DOA of the acoustic waves being emitted by the ASC and arriving at the AUV USBL system is given by

$$\mathbf{d}_s(t) = \frac{\mathbf{r}_s(t)}{\rho(t)}, \tag{7}$$

where $\rho(t) \in \mathbb{R}$ is the distance between the ASC and the AUV, i.e., $\rho(t) = \|\mathbf{r}_s(t)\|$. The direction vector $\mathbf{d}_s(t) \in S(2)$ is unitary by definition and is considered to be measured by the USBL device installed on-board the AUV.

Differentiating (7) in time yields

$$\dot{\mathbf{d}}_s(t) = \frac{\dot{\mathbf{r}}_s(t)\rho(t) - \mathbf{r}_s(t)\dot{\rho}(t)}{\rho^2(t)}. \tag{8}$$

The time derivative of the range $\rho(t)$ in (8) is simply given by

$$\dot{\rho}(t) = \frac{1}{\rho(t)}\mathbf{r}_s(t)^T\dot{\mathbf{r}}_s(t). \tag{9}$$

Taking into account that $\mathbf{d}_s \cdot (\boldsymbol{\omega} \times \mathbf{d}_s) = \mathbf{0}$ and substituting (5) and (9) in (8) yields

$$\dot{\mathbf{d}}_s(t) = -\mathcal{S}\left[\boldsymbol{\omega}(t)\right]\mathbf{d}_s(t) + \frac{\mathbf{v}_\mathbf{r}(t)}{\rho(t)} + \mathbf{d}_s(t)\mathbf{d}_s^T(t)\frac{\mathbf{v}_\mathbf{r}(t)}{\rho(t)}. \tag{10}$$

Exploiting the cross-product multiplication property that asserts $\mathcal{S}\left[\mathbf{a}\right]\mathcal{S}\left[\mathbf{a}\right] = \mathbf{a}\mathbf{a}^T - \|\mathbf{a}\|^2\mathbf{I}_3$, and the fact that $\|\mathbf{d}_s(t)\| = 1$ by definition, it is possible to simplify (10) as

$$\dot{\mathbf{d}}_s(t) = -\mathcal{S}\left[\boldsymbol{\omega}(t)\right]\mathbf{d}_s(t) - \mathcal{S}^2\left[\mathbf{d}_s(t)\right]\mathbf{u}(t), \tag{11}$$

where

$$\mathbf{u}(t) = \frac{\mathbf{v}_\mathbf{r}(t)}{\rho(t)} \tag{12}$$

is regarded as the system input.

### 2.2 Gravity reading vector observation

The second vector observation is drawn from the gravity vector that is present in the accelerometers readings. As carefully discussed in [20], for sufficient low frequency bandwidths, the gravitational field dominates the accelerometer readings in body-fixed coordinates. The gravity vector is a locally constant vector quantity in inertial coordinates, thus making it a feasible vector measurement for attitude estimation purposes. Thus, the gravity vector is represented in AUV body-fixed coordinates as

$$\mathbf{g}(t) = \mathcal{R}_u(t)^T\,{}^I\mathbf{g}, \tag{13}$$

where ${}^I\mathbf{g} \in \mathbb{R}^3$ is the gravity vector in inertial coordinates, and its time derivative is simply given by

$$\dot{\mathbf{g}}(t) = -\mathcal{S}\left[\boldsymbol{\omega}(t)\right]\mathbf{g}(t). \tag{14}$$

## 3 Filter design

This section presents the design of a filtering solution for the estimation of the attitude of the AUV, merging the vector observations presented in Section 2 in a combined dual vector observer setting, and extracting the attitude information from the estimated vector observations. Specifically, the combined dual vector observer framework is brought to full detail in Section 3.1, whereas the filtering solution is presented in Section 3.2.

### 3.1 Combined dual vector observer

Combining (11) and (14) yields

$$\begin{cases} \dot{\mathbf{d}}_s(t) = & -\mathcal{S}\left[\boldsymbol{\omega}(t)\right]\mathbf{d}_s(t) - \mathcal{S}^2\left[\mathbf{d}_s(t)\right]\mathbf{u}(t) \\ \dot{\mathbf{g}}(t) = & -\mathcal{S}\left[\boldsymbol{\omega}(t)\right]\mathbf{g}(t) \\ \mathbf{y}_1(t) = & \mathbf{d}_s(t) \\ \mathbf{y}_2(t) = & \mathbf{g}(t) \end{cases}, \tag{15}$$

where $\mathbf{y}_1(t)$ and $\mathbf{y}_2(t)$ are the outputs of the system: $\mathbf{y}_1(t) = \mathbf{d}_s(t)$ is measured by the USBL device and $\mathbf{y}_2(t) = \mathbf{g}(t)$ is obtained from the low-frequency content in the accelerometer readings.

Considering that the rate gyros readings (4) are corrupted by constant biases in (15) yields

$$\begin{cases} \dot{\mathbf{d}}_s(t) = & -\mathcal{S}\left[\boldsymbol{\omega}_m(t)\right]\mathbf{d}_s(t) + \mathcal{S}\left[\mathbf{b}_{\boldsymbol{\omega}}(t)\right]\mathbf{d}_s(t) - \mathcal{S}^2\left[\mathbf{d}_s(t)\right]\mathbf{u}(t) \\ \dot{\mathbf{g}}(t) = & -\mathcal{S}\left[\boldsymbol{\omega}_m(t)\right]\mathbf{g}(t) + \mathcal{S}\left[\mathbf{b}_{\boldsymbol{\omega}}(t)\right]\mathbf{g}(t) \\ \dot{\mathbf{b}_{\boldsymbol{\omega}}}(t) = & \mathbf{0} \\ \mathbf{y}_1(t) = & \mathbf{d}_s(t) \\ \mathbf{y}_2(t) = & \mathbf{g}(t) \end{cases}. \tag{16}$$

Using the cross-product property $\boldsymbol{\omega} \times \mathbf{a} = -\mathbf{a} \times \boldsymbol{\omega}$ and the considered outputs, (16) can be regarded as a linear time-varying (LTV) system, even though it is still nonlinear (see [5, Lemma 1]). Thus, it comes

$$\begin{cases} \dot{\mathbf{x}}(t) = & \mathbf{A}(t)\mathbf{x}(t) + \mathbf{B}(t)\mathbf{u}(t) \\ \mathbf{y}(t) = & \mathbf{C}\mathbf{x}(t) \end{cases}, \tag{17}$$

where $\mathbf{x}(t) = \begin{bmatrix}\mathbf{d}_s^T(t) & \mathbf{g}^T(t) & \mathbf{b}_{\boldsymbol{\omega}}^T(t)\end{bmatrix}^T$ is the system state,

$$\mathbf{A}(t) = \begin{bmatrix} -\mathcal{S}\left[\boldsymbol{\omega}_m(t)\right] & \mathbf{0}_{3\times3} & -\mathcal{S}\left[\mathbf{y}_1(t)\right] \\ \mathbf{0}_{3\times3} & -\mathcal{S}\left[\boldsymbol{\omega}_m(t)\right] & -\mathcal{S}\left[\mathbf{y}_2(t)\right] \\ \mathbf{0}_{3\times3} & \mathbf{0}_{3\times3} & \mathbf{0}_{3\times3} \end{bmatrix} \in \mathbb{R}^{9\times9},$$
$$\mathbf{B}(t) = \begin{bmatrix} -\mathcal{S}^2\left[\mathbf{y}_1(t)\right] & \mathbf{0}_{3\times3} & \mathbf{0}_{3\times3} \end{bmatrix}^T \in \mathbb{R}^{9\times3},$$

and

$$\mathbf{C} = \begin{bmatrix} \mathbf{I}_3 & \mathbf{0}_{3\times3} & \mathbf{0}_{3\times3} \\ \mathbf{0}_{3\times3} & \mathbf{I}_3 & \mathbf{0}_{3\times3} \end{bmatrix} \in \mathbb{R}^{6\times9}.$$

Before proceeding with the observability analysis of (17), the following lemma is introduced.

**Lemma 1** *Let $\mathbf{f}(t) : [t_0, t_f] \subset \mathbb{R} \to \mathbb{R}^n$ be a continuous and two times continuously differentiable function on $\mathcal{I} := [t_0, t_f]$, $T := t_f - t_0 > 0$, and such that $\mathbf{f}(t_0) = \mathbf{0}$. Further assume that $\max_{t\in\mathcal{I}} \|\ddot{\mathbf{f}}(t)\| \leq C$. If there exists a constant $\alpha^* > 0$ and a time instant $t^* \in \mathcal{I}$ such that $\|\dot{\mathbf{f}}(t^*)\| \geq \alpha^*$, then there exist constants $\beta^* > 0$ and $0 < \delta^* \leq T$ such that $\|\mathbf{f}(t_0 + \delta^*)\| \geq \beta^*$.*

**Proof** This Lemma is a particular case of [4, Proposition 4.2].

The observability analysis of (17) is addressed in the following theorem.

**Theorem 2** *If the AUV is never exactly below the ASC, such that the gravity vector and the USBL direction vector are not parallel, i.e.*

$$\mathbf{d}_s(t) \times \mathbf{g}(t) \neq \mathbf{0}, \tag{18}$$

*then the pair* $(\mathbf{A}(t), \mathbf{C})$ *is uniformly completely observable (UCO) [26], that is, there exist positive constants* $\alpha_1$*,* $\alpha_2$*, and* $\delta$ *such that*

$$\alpha_1 \mathbf{I} \preceq \boldsymbol{\mathcal{W}}(t, t+\delta) \preceq \alpha_2 \mathbf{I}$$

*for all* $t \geq t_0$*, where* $t_0$ *is some initial time instant, and* $\boldsymbol{\mathcal{W}}(t, t+\delta)$ *is the observability Gramian associated with the pair* $(\mathbf{A}(t), \mathbf{C})$ *on* $[t, t+\delta]$*.*

**Proof** Let $\mathcal{R}_m \in SO(3)$ be a rotation matrix such that

$$\dot{\mathcal{R}}_m(t) = \mathcal{R}_m(t)\mathcal{S}\left[\boldsymbol{\omega}_m(t)\right],$$

where $\boldsymbol{\omega}_m(t)$ is the bias-corrupted rate gyros measurements, and consider the state transformation $\mathbf{z}(t) = \mathbf{T}(t)\mathbf{x}(t)$, with $\mathbf{T}(t) = \mathrm{diag}(\mathcal{R}_m(t), \mathcal{R}_m(t), \mathbf{I}_3)$, which is a Lyapunov state transformation and therefore preserves observability properties [9]. Straightforward computations yield the new system dynamics

$$\begin{cases} \dot{\mathbf{z}}(t) = & \mathcal{A}(t)\mathbf{z}(t) + \mathcal{B}(t)\mathbf{u}(t) \\ \mathbf{y}(t) = & \mathcal{C}(t)\mathbf{z}(t) \end{cases}.$$

where $\mathbf{z}(t) = \begin{bmatrix} \mathbf{z}_1^T(t) & \mathbf{z}_2^T(t) & \mathbf{b}_{\boldsymbol{\omega}}^T(t) \end{bmatrix}^T$ is the system state, with $\mathbf{z}_1(t), \mathbf{z}_2(t) \in \mathbb{R}^3$,

$$\mathcal{A}(t) = \begin{bmatrix} \mathbf{0}_{3\times3} & \mathbf{0}_{3\times3} & -\mathcal{R}_m(t)\mathcal{S}\left[\mathbf{y}_1(t)\right] \\ \mathbf{0}_{3\times3} & \mathbf{0}_{3\times3} & -\mathcal{R}_m(t)\mathcal{S}\left[\mathbf{y}_2(t)\right] \\ \mathbf{0}_{3\times3} & \mathbf{0}_{3\times3} & \mathbf{0}_{3\times3} \end{bmatrix} \in \mathbb{R}^{9\times9},$$
$$\mathcal{B}(t) = \begin{bmatrix} -\mathcal{S}^2\left[\mathbf{y}_1(t)\right]\mathcal{R}_m^T(t) & \mathbf{0}_{3\times3} & \mathbf{0}_{3\times3} \end{bmatrix}^T \in \mathbb{R}^{9\times3},$$

and

$$\mathcal{C}(t) = \begin{bmatrix} \mathcal{R}_m^T(t) & \mathbf{0}_{3\times3} & \mathbf{0}_{3\times3} \\ \mathbf{0}_{3\times3} & \mathcal{R}_m^T(t) & \mathbf{0}_{3\times3} \end{bmatrix} \in \mathbb{R}^{6\times9}.$$

The state transition matrix $\Phi(\tau, t)$ for this particular system is simply given by

$$\Phi(\tau, t) = \mathbf{I}_9 + \int_t^\tau \mathcal{A}(\sigma)d\sigma. \tag{19}$$

The bounds on the observability Gramian $\boldsymbol{\mathcal{W}}(t, t+\delta)$ can be written as

$$\alpha_1 \leq \mathbf{a}^T\boldsymbol{\mathcal{W}}(t, t+\delta)\mathbf{a} \leq \alpha_2, \tag{20}$$

for all $t \geq t_0$ and $\mathbf{a} \in \{\mathbf{x} \ \in \mathcal{R}^9 : \ \|\mathbf{x}\| = 1\}$. The observability Gramian associated with the pair $(\mathcal{A}(t), \mathcal{C}(t))$ on $[t, t+\delta]$ is defined by [1]

$$\boldsymbol{\mathcal{W}}(t, t+\delta) = \int_t^{t+\delta} \Phi(\tau, t)^T \mathcal{C}^T(\tau) \mathcal{C}(\tau) \Phi(\tau, t) d\tau. \tag{21}$$

Thus, the observability Gramian (20) bounds can be rewritten as

$$\alpha_1 \leq \int_t^{t+\delta} \|\mathbf{f}(\tau, t)\|^2 d\tau \leq \alpha_2, \tag{22}$$

where

$$\mathbf{f}(\tau, t) := \mathcal{C}(\tau) \Phi(\tau, t) \mathbf{a}, \tag{23}$$

for all $t \geq t_0$, $\tau \in [t, t+\delta]$. The existence of the upper bound $\alpha_2$ on (22) is easily seen to be always satisfied, since $\mathcal{A}(t)$ and $\mathcal{C}(\tau)$ are continuous norm-bounded matrices. It remains to show that (22) is lower bounded by a positive constant $\alpha_1$ for all $t \geq t_0$. Let $\mathbf{a}_1, \ \mathbf{a}_2, \ \mathbf{a}_3 \in \mathcal{R}^3$. Setting $\mathbf{a} = \begin{bmatrix} \mathbf{a}_1^T & \mathbf{a}_2^T & \mathbf{a}_3^T \end{bmatrix}^T$ in (23) and taking into account (19) yields

$$\mathbf{f}(\tau, t) = \begin{bmatrix} \mathbf{a}_1 - \int_t^\tau \mathcal{R}_m(\sigma) \mathcal{S}\left[\mathbf{y}_1(\sigma)\right] \mathbf{a}_3 d\sigma \\ \mathbf{a}_2 - \int_t^\tau \mathcal{R}_m(\sigma) \mathcal{S}\left[\mathbf{y}_1(\sigma)\right] \mathbf{a}_3 d\sigma \end{bmatrix}. \tag{24}$$

Evaluating (24) at $\tau = t$, the integral term is null and it is straightforward to verify that if $\mathbf{a}_1 \neq \mathbf{0}$ or $\mathbf{a}_2 \neq \mathbf{0}$ then $\|\mathbf{f}(t, t)\|$ is immediately bounded from below as

$$\|\mathbf{f}(t, t)\| \geq \|\mathbf{a}_1\| = \alpha_1^*, \qquad \text{if } \mathbf{a}_1 \neq \mathbf{0}, \tag{25}$$

or

$$\|\mathbf{f}(t, t)\| \geq \|\mathbf{a}_2\| = \alpha_2^*, \qquad \text{if } \mathbf{a}_2 \neq \mathbf{0} \tag{26}$$

for all $t \geq t_0$. However, if $\mathbf{a}_1 = \mathbf{a}_2 = \mathbf{0}$ it follows that $\mathbf{f}(t, t) = \mathbf{0}$, $\|\mathbf{a}_3\| = 1$, and

$$\frac{\partial \mathbf{f}}{\partial \tau}(\tau, t) = - \begin{bmatrix} \mathcal{R}_m(\tau) \mathcal{S}\left[\mathbf{y}_1(\tau)\right] \mathbf{a}_3 \\ \mathcal{R}_m(\tau) \mathcal{S}\left[\mathbf{y}_2(\tau)\right] \mathbf{a}_3 \end{bmatrix}. \tag{27}$$

Evaluating (27) at $\tau = t$ yields

$$\left.\frac{\partial \mathbf{f}}{\partial \tau}(\tau, t)\right|_{\tau = t} = - \begin{bmatrix} \mathcal{R}_m(t) \mathcal{S}\left[\mathbf{y}_1(t)\right] \mathbf{a}_3 \\ \mathcal{R}_m(t) \mathcal{S}\left[\mathbf{y}_2(t)\right] \mathbf{a}_3 \end{bmatrix}. \tag{28}$$

Suppose now that (18) is true, that is $\mathbf{y}_1(t) \times \mathbf{y}_2(t) \neq \mathbf{0}$. Then there exists $\alpha_3^* > 0$ such that

$$\left\| \left.\frac{\partial \mathbf{f}}{\partial \tau}(\tau, t)\right|_{\substack{\tau = t \\ \mathbf{a}_1 = \mathbf{0} \\ \mathbf{a}_2 = \mathbf{0}}} \right\| \geq \alpha_3^* > 0, \tag{29}$$

for all $t \geq t_0$. Using Lemma 1 with (29) comes that there exist $\alpha_4^* > 0$ and $\delta_1^* > 0$ such that

$$\|\mathbf{f}(t + \delta_1^*, t)\| \geq \alpha_4^*, \tag{30}$$

for all $t \geq t_0$. Finally, using Lemma 1 again comes that there exist $\alpha > 0$ and $\delta > 0$ such that

$$\mathbf{a}^T \boldsymbol{\mathcal{W}}(t, t+\delta)\mathbf{a} \geq \alpha > 0 \tag{31}$$

for all $t \geq t_0$ and for all $\mathbf{a} \in \{\mathbf{x} \in \mathcal{R}^9 : \|\mathbf{x}\| = 1\}$, which means that the pair $(\mathcal{A}(t), \mathcal{C})$ is uniformly completely observable, and consequently means that the pair $(\mathbf{A}(t), \mathbf{C})$ is also uniformly completely observable (see [5, Lemma 1]) and therefore concludes the proof.

**Remark 3** *Notice that, by definition, the ASC (surface craft) is never below the AUV (underwater vechicle), thus in practice, what Theorem 2 states is that if the AUV does not navigate directly under the ASC, then the pair* $(\mathbf{A}(t), \mathbf{C})$ *is uniformly completely observable.*

**Remark 4** *Theorem 2 provides only sufficient conditions for the pair* $(\mathbf{A}(t), \mathbf{C})$ *to be UCO. The system might still be UCO even if the vectors are parallel, requiring however some persistent excitation conditions on angular motion of the vehicle [3].*

Albeit other filtering solutions such as $H_\infty$ could be devised, the design of a Kalman Filter with globally asymptotically stable error dynamics follows simply by including state and observation disturbances $\mathbf{n_x}(t)$ and $\mathbf{n_y}(t)$

$$\begin{cases} \dot{\mathbf{x}}(t) = & \mathbf{A}(t)\mathbf{x}(t) + \mathbf{B}(t)\mathbf{u}(t) + \mathbf{n_x}(t) \\ \mathbf{y}(t) = & \mathbf{C}\mathbf{x}(t) + \mathbf{n_y}(t) \end{cases}, \tag{32}$$

which are considered to be uncorrelated additive white Gaussian noise (AWGN) with covariance matrices given by

$$E[\mathbf{n_x}(t)\mathbf{n_x}(\tau)^T] = \mathbf{Q}(t)\delta(t-\tau), \tag{33}$$

$$E[\mathbf{n_y}(t)\mathbf{n_y}(\tau)^T] = \mathbf{R}(t)\delta(t-\tau), \tag{34}$$

respectively. Additional states could be added to model the observation and process disturbances as colored noise, by modelling $\mathbf{n_x}(t)$ and $\mathbf{n_y}(t)$ as outputs of stable linear time-invariant filters. Nonetheless, the resulting Kalman filter equations are standard [13] and therefore omitted.

## 3.2 Attitude estimation

The filtering architecture presented so far allows for the AUV to filter the noisy gravity and USBL direction vector measurements and obtain accurate body-fixed estimates of two vectors while estimating the rate gyros biases with an optimal filter with GAS properties. In this section, an attitude solution is derived from the two proposed filtered vector measurements, exploiting the tandem vehicle formation and the ability to exchange information through acoustic modems.

Taking into account that

$$\|\mathbf{r}_s(t)\| = \|\mathbf{r}_u(t)\| = \rho(t)$$

it comes from (2) that the direction of the AUV measured on the ASC vehicle is given by

$$\mathbf{d}_u(t) = \frac{\mathbf{r}_u(t)}{\rho(t)} = \mathcal{R}_s^T(t)\frac{\mathbf{p}_u(t) - \mathbf{p}_s(t)}{\rho(t)}. \tag{35}$$

Now, let

$${}^{I}\mathbf{d}_u(t) = \frac{\mathbf{p}_u(t) - \mathbf{p}_s(t)}{\rho(t)}. \tag{36}$$

Using (36) it is immediate to see that (35) can be written as

$$\mathbf{d}_u(t) = \mathcal{R}_s^T(t)\,{}^{I}\mathbf{d}_u(t), \tag{37}$$

and the ASC direction measured in the AUV coordinate frame comes as

$$\mathbf{d}_s(t) = \mathcal{R}_u^T(t)\,{}^{I}\mathbf{d}_s(t) = \mathcal{R}_u^T(t)(-\,{}^{I}\mathbf{d}_u(t)), \tag{38}$$

where ${}^{I}\mathbf{d}_s(t) = -\,{}^{I}\mathbf{d}_u(t)$ is the natural inertial reference for the AUV body-fixed USBL measurement. For vehicles working in tandem, as in the case of the framework proposed herein, this quantity is invariant to rotations and can be considered slowly time-varying for attitude estimation purposes.

Since the ASC vehicle is navigating on the sea surface, and benefits from the availability of GPS signals, it is considered to have a complete navigation package, which provides accurate inertial velocity and attitude and heading estimates. Thus it is able to invert its own USBL measurements as $\hat{\mathcal{R}}_s(t)\mathbf{d}_u(t)$ and send it to the AUV via the acoustic modem link in order to aid the underwater vehicle attitude estimation algorithm. In the proposed architecture, depicted in Fig. 4, the surface vehicle sends to the underwater vehicle, via acoustic modem, the estimates of its own inertial velocity ${}^{I}\mathbf{v}_{ASC}(t)$, the direction vector ${}^{I}\mathbf{d}_u(t)$, and the range $\rho(t)$, which is computed from either the USBL tracking scheme or from the acoustic modem itself.

The optimal attitude estimation solution, in a least-squares sense, is obtained from the minimization of the cost functional

$$J(\mathcal{R}) = \frac{1}{2}\sum_{i=1}^{N} a_i \left\|\mathbf{y}_i - \mathcal{R}^T\,{}^{I}\mathbf{y}_i\right\|^2, \tag{39}$$

which is commonly known in the literature as the Wahba's problem [31], and where the weighting parameter $a_i$ can be chosen to reflect the confidence on each sensor. For the case of more than one non-collinear vector observation, that is $N \geq 2$ in (39), there exists a closed-loop solution [21, 22], based on the singular value decomposition (SVD) [29].

Let

$$\mathbf{B} = \sum_{i=1}^{N} \bar{\mathbf{y}}_i\,{}^{I}\bar{\mathbf{y}}_i^T, \quad \in \mathbb{R}^{3\times 3}, \tag{40}$$

where $\bar{\mathbf{y}}_i$ represents the normalized filtered estimates from (32)

$$\bar{\mathbf{y}}_1 = \frac{\mathbf{y}_1}{\|\mathbf{y}_1\|}, \quad \bar{\mathbf{y}}_2 = \frac{\mathbf{y}_2}{\|\mathbf{y}_2\|}, \tag{41}$$

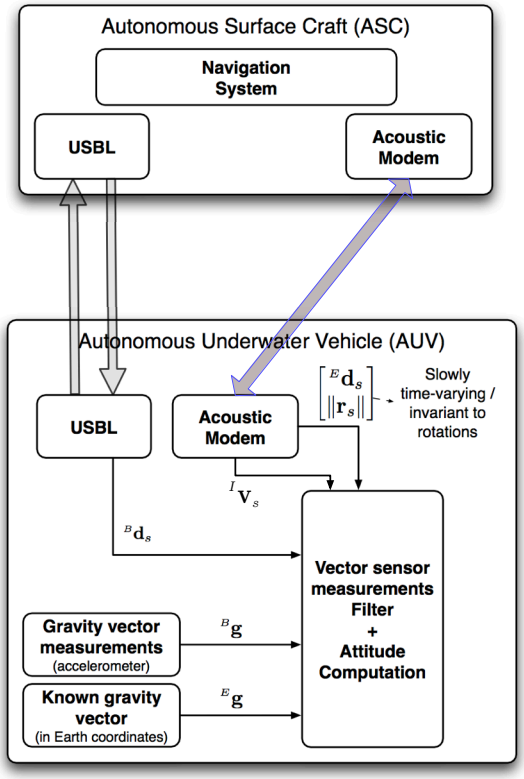


Figure 4: Proposed tandem architecture

and ${}^{I}\bar{\mathbf{y}}_i$ the corresponding inertial representations

$$ {}^{I}\bar{\mathbf{y}}_1 = \frac{{}^{I}\mathbf{y}_1}{\| {}^{I}\mathbf{y}_1 \|}, \quad {}^{I}\bar{\mathbf{y}}_2 = \frac{{}^{I}\mathbf{y}_2}{\| {}^{I}\mathbf{y}_2 \|}, \tag{42} $$

and consider the SVD decomposition [29]

$$ \mathbf{B} = \mathbf{U}\boldsymbol{\Sigma}\mathbf{V}^T, \tag{43} $$

where $\mathbf{U}$ and $\mathbf{V}$ are unitary matrices, and $\boldsymbol{\Sigma}$ is a diagonal matrix that contains the singular values of $\mathbf{B}$.

Thus, the optimal solution for $\mathcal{R}$ that minimizes (39), presented in [22] and provided here for completeness, is computed as

$$ \mathcal{R}^T = \mathbf{U} \begin{bmatrix} 1 & 0 & 0 \\ 0 & 1 & 0 \\ 0 & 0 & \det(\mathbf{U})\det(\mathbf{V}) \end{bmatrix} \mathbf{V}^T. \tag{44} $$

Based on the information received through the acoustic modem, the AUV computes the relative velocity $\mathbf{v}_{\mathbf{r}}(t)$ from (6) as

$$\mathbf{v}_{\mathbf{r}}(t) = \hat{\mathcal{R}}_u^T(t)\, {}^I\mathbf{v}_s(t) - \mathbf{v}_u(t), \tag{45}$$

where the underwater vehicle velocity $\mathbf{v}_u(t) \in \mathbb{R}^3$ is measured by the on-board DVL, and $\hat{\mathcal{R}}_u(t) \in SO(3)$ is an *a priori* estimate for the rotation matrix $\mathcal{R}_u(t)$, computed from the available noisy measurements. The received range $\rho(t)$ is used with (45) to compute the system input $\mathbf{u}(t)$ in (12), and drive the sensor-based vector measurement filter dynamics (32). Finally, the filtered attitude estimate is computed *a posteriori*, using the optimal solution from (44) with the filtered vectors.

**Remark 5** *The attitude solution computed from* (44) *is not well defined for a set of parallel vectors. It might happen by accident that the estimated vectors* $\hat{\mathbf{y}}_1(t^*)$ *and* $\hat{\mathbf{y}}_2(t^*)$ *are parallel, that is* $\hat{\mathbf{y}}_1(t^*) \times \hat{\mathbf{y}}_2(t^*) = 0$*, or null for some time* $t^*$*, as in the filtering structure presented herein, there are no restrictions imposed on the cross-product* $\hat{\mathbf{y}}_1(t) \times \hat{\mathbf{y}}_2(t)$*. However, if such happens in practice during the initial convergence of the filter for instance, an attitude solution can be computed directly from the vector sensor measurements. Nonetheless, sustained on the GAS properties of the error dynamics the filter is guaranteed to converge, and as it will be shown in Section 4, the proposed architecture exhibits very fast convergence, of less than one second.*

# 4 Numerical results and performance evaluation

The proposed solution is evaluated in this section resorting to extensive Monte-Carlo numerical simulations of two autonomous vehicles, operating in a typical survey and intervention scenario. The vehicles describe a trajectory as depicted in Fig. 5, in which both the ASC and the AUV start heading north along the x-axis at the same speed, and then the AUV identifies an intervention target and descends on a helicoidal trajectory while the ASC waits for it to complete its descent. When the AUV reaches the bottom, both vehicles travel northbound before performing a coordinated 180-degree turn and return to the origin of the mission. The motion of both vehicles is performed on an higher-layer of the mission controllers, coordinated via the on-board acoustic modems. The ASC, as it navigates on the surface, is affected by the sea state and thus its nominal position and velocity are disturbed by the motion of the waves.

Both vehicles are equipped with acoustic modems and USBL positioning devices, whereas the ASC USBL unit is mounted in a standard surface-mount scheme, whilst the AUV USBL unit is mounted in what is known as an inverted-USBL configuration [30]. Table 1 summarizes the sensor packages of each vehicle. The acoustic modems are also able to provide range measurements between the two vehicles via handshaking protocols, and, due to environmental restrictions such as a low underwater sound propagation velocity and harsh multipath conditions, have considerable bandwidth limitations and message delivery delays. In particular, with a nominal underwater sound speed of $1515\ ms^{-1}$, and due to the distances considered between the two vehicles (in

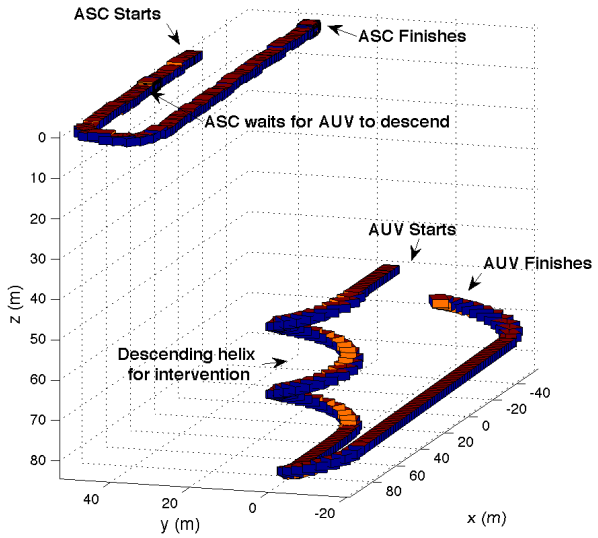


Figure 5: Vehicles trajectory

the trajectory described in Fig. 5) the messages sent from the ASC to the AUV are only delivered after the propagation delay profiled in Fig. 6. The limited bandwidth of the acoustic modems is also taken into consideration in the simulations presented herein: the ASC needs to send messages to the AUV with a payload composed of the inertial reference direction vector ${}^{I}\mathbf{d}_{s}(t)$ and the ASC inertial velocity ${}^{I}\mathbf{v}_{s}$. Even though message compression techniques can be employed, the worst case scenario is to send without compression three single-precision floating point numbers (32 bit floats) for each vector quantity, which implies a payload of 192 bits per message. Commercially available acoustic modems such as the Link-Quest® UWM2000 have payload data rates of 6600 bits per second (bps). Thus, in addition to delivery delays and to keep the simulations realistic, the acoustic modems are considered to successfully transmit only ten (10) messages per second, which reserves a bandwidth of 1920 bps for the required communications. The quantities being transmitted over the acoustic link are, nonetheless, invariant to rotations of the AUV, and can be considered slowly time-varying for attitude estimation purposes. Moreover, if significant packets losses occur in practice, the navigation algorithms can still provide attitude estimates by numerically integrating the rate gyros outputs, which are now properly compensated for bias using the bias estimation capabilities of the filter presented herein. Enhanced numerical integration algorithms for attitude are available in the literature, see [15] and [27], that require nonetheless proper bias compensation of the rate gyros outputs, and their usage are a common practice in the navigation of real world underwater vehicles [19, 8].

All the sensors installed on-board the AUV are considered to be disturbed by additive white Gaussian noise, as described on Table 2, while the ASC navigation package

Table 1: Vehicles sensor packages

| | **Vehicle** | |
|---|---|---|
| **Sensor package** | **ASC** (surface) | **AUV** (underwater) |
| Full navigation state (INS) | **Yes** | **No** |
| GPS | **Yes** | **No**: unavailable underwater |
| USBL | **Yes**: standard surface mount | **Yes**: inverted configuration |
| DVL | - | **Yes**: with bottom-lock |
| Magnetometer | - | **No**: unavailable due to strong environmental magnetic distortions during intervention |
| Rate gyros | (included in INS) | **Yes**: corrupted with biases |
| Accelerometers | (included in INS) | **Yes**: used as gravitometer |
| Acoustic Modem | **Yes** | **Yes** |

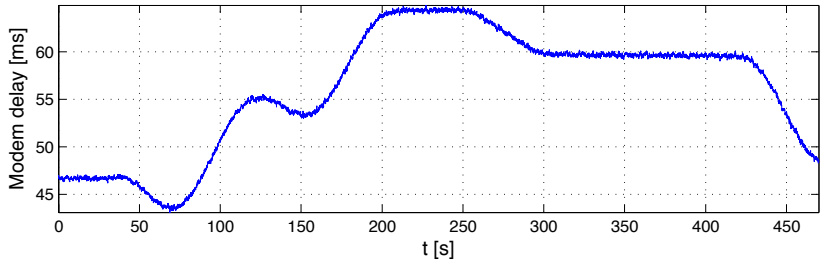

Figure 6: Modem communications time delay profile

provides measurements with an accuracy described by the AWGN described in Table 3. The Kalman filter gains were adjusted to allow for a fast convergence with

$$\mathbf{R}(t) = \text{diag}\left(10^{-3}\mathbf{1}_{3\times1}, 10^{-3}\mathbf{1}_{3\times1}\right),$$
$$\mathbf{Q}(t) = \text{diag}\left(10^{-5}\mathbf{1}_{3\times1}, 10^{-5}\mathbf{1}_{3\times1}, 10^{-7}\mathbf{1}_{3\times1}\right),$$

and maintain good steady-state performance when compared to the raw attitude measurement, obtained by minimizing (39) with the unfiltered vector measurements.

The filter performance is evaluated in simulation resorting to one thousand (1000) Monte-Carlo runs, in which the sensors are affected by different noise sequences with the standard deviations specified in Tables 2 and 3, and the filter is exposed to several

Table 2: AUV sensors noise characteristics

| On-board Sensor | AWGN Standard deviation |
|---|---|
| Rate gyros | $0.05\ [deg\ s^{-1}]$ |
| DVL velocity | $1\ [mm\ s^{-1}]$ |
| USBL azimuth | $0.5\ [deg]$ |
| USBL elevation | $0.5\ [deg]$ |
| Accelerometer | $1\ [mg]$ |
| Range | $1\ [m]$ |

Table 3: ASC estimates AWGN standard deviation

| On-board Sensor | AWGN Standard deviation |
|---|---|
| AHRS yaw | $0.1\ [deg]$ |
| AHRS pitch | $0.01\ [deg]$ |
| AHRS roll | $0.01\ [deg]$ |
| Velocity | $1\ [mm\ s^{-1}]$ |
| USBL filtered azimuth | $0.05\ [deg]$ |
| USBL filtered elevation | $0.05\ [deg]$ |

initial conditions. To generate the initial conditions for the filter, the nominal gravity and direction vectors are rotated according to an initial attitude error drawn from a normal distribution with a standard deviation of $180$, $45$, and $20\ deg$ in yaw, pitch, and roll respectively. The initial rate gyro bias estimate was set to zeros whilst the nominal bias was $[5,\ -3,\ 4]\ deg\ s^{-1}$. The fast convergence of less than one second is evidenced from the estimation error plots in Fig. 7 for the USBL direction, and in Fig. 8 for the gravity vector. The linear acceleration $\dot{\mathbf{v}}(t)$ of the vehicle present on the accelerometers readings is seen to cause some disturbances on the gravity vector estimation error in Fig. 8 as this quantity was not modelled in the original state space. This disturbance is expected, even in classical attitude filters that use accelerometers to provide gravity measurements, when the linear acceleration of the vehicle also affects the low-frequency content of the accelerometer measurements. The overall filtered attitude estimate is compared to the raw attitude measurements in Fig. 9. The estimation of the rate gyros biases also exhibits a fast convergence as evidenced in Fig. 10.

# 5 Conclusions

This paper presented a novel approach to the design of an attitude filter for an I-AUV, navigating in tandem with a surface craft. In the proposed framework, the ASC aids the I-AUV determine its attitude, by providing an inertial reference direction vector through acoustic modem communications, which is measured in body-fixed coordinates by an Ultra-Short Baseline (USBL) device. Magnetometers are avoided in the

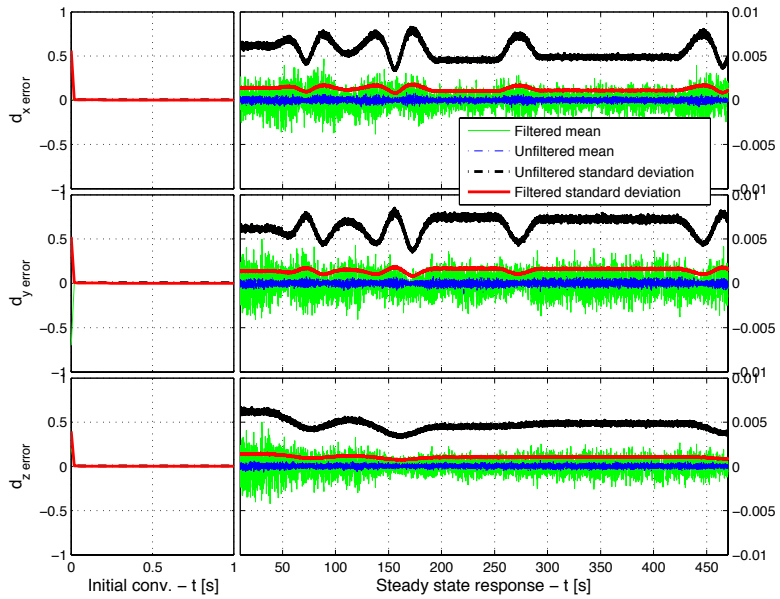


Figure 7: USBL direction vector estimation error (1000 Monte-Carlo runs)

solution that was proposed, due to space anomalies and magnetic distortions that are introduced by intervention targets that may include Man-made objects, large metal structures, and ship wrecks that have strong magnetic signatures. The filtering architecture presented herein includes the estimation of rate gyros biases, which is a fundamental feature for open-loop integration of the vector kinematics. A modification of the system dynamics allows for the nonlinear system to be regarded as an LTV, still being nonetheless nonlinear. An observability analysis is conducted using this modified system showing it to be uniformly completely observable, under some mild restrictions on the tandem vehicle configuration. This allows for the design of a standard Kalman filter with GAS error dynamics. The feasibility of the proposed architecture was assessed resorting to extensive Monte-Carlo numerical simulations with realistic sensor noise, considering also adequate communications delays and limited bandwidth of the acoustic modems, and its performance was shown to yield very satisfactory results. Future work on this subject will focus on the real-time implementation of the proposed architecture within the scope of the EU project TRIDENT.

# Acknowledgements

This work was partially supported by Fundação para a Ciência e a Tecnologia (ISR/IST plurianual funding), by the project FCT PTDC/EEA-CRO/111197/2009 - MAST/AM of the FCT, and by the EU Project TRIDENT (Contract No. 248497). The work of Marco Morgado was supported by PhD Student Scholarship SFRH/BD/25368/2005

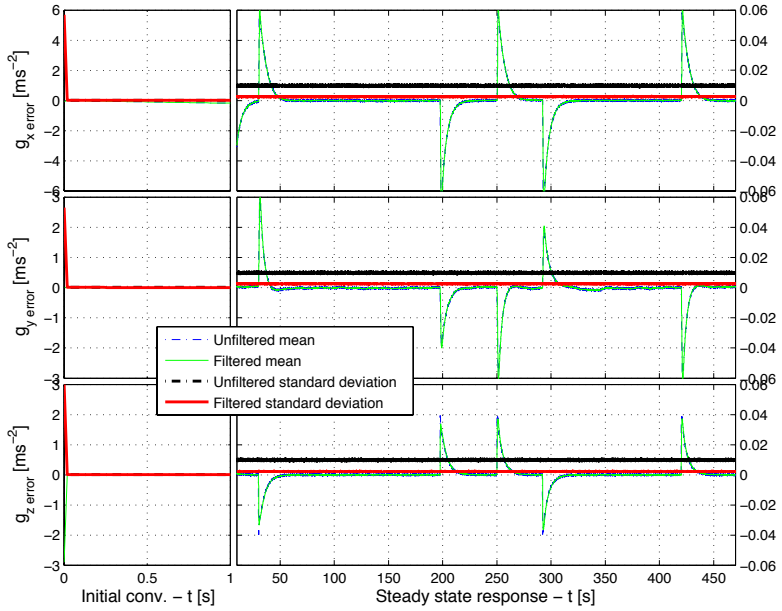


Figure 8: Gravity vector estimation error (1000 Monte-Carlo runs)

from the Portuguese FCT POCTI programme.

# References

[1] P.J. Antsaklis and A.N. Michel. *Linear systems*. Birkhauser, 2006.

[2] I.Y. Bar-Itzhack and Y. Oshman. Attitude determination from vector observations: Quaternion estimation. *Aerospace and Electronic Systems, IEEE Transactions on*, AES-21(1):128 –136, January 1985.

[3] P. Batista, C. Silvestre, and P. Oliveira. Sensor-based Complementary Globally Asymptotically Stable Filters for Attitude Estimation. In *Proceedings of the 48th IEEE Conference on Decision and Control*, pages 7563–7568, Shanghai, China, December 2009.

[4] P. Batista, C. Silvestre, and P. Oliveira. On the observability of linear motion quantities in navigation systems. *Systems & Control Letters*, 60(2):101 – 110, 2011.

[5] P. Batista, C. Silvestre, and P. Oliveira. Single Range Aided Navigation and Source Localization: observability and filter design. *Systems & Control Letters*, 60(8):665–673, August 2011.

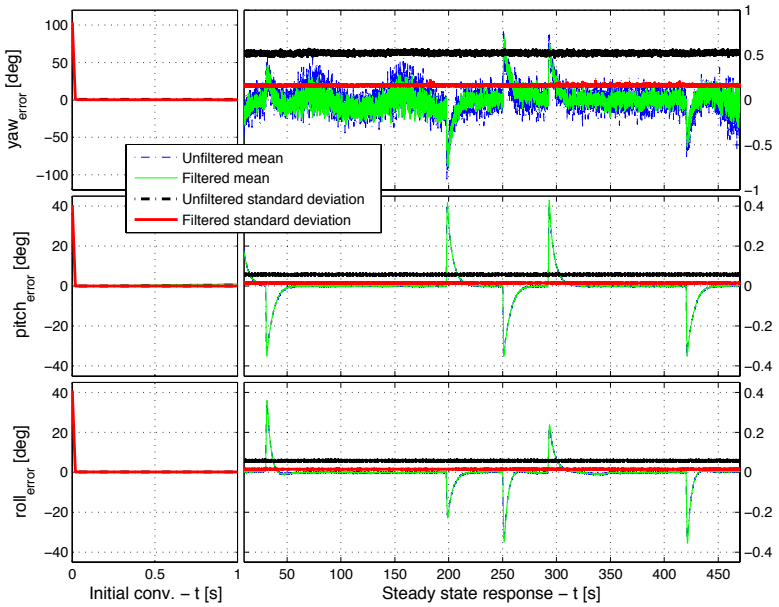


Figure 9: Attitude estimation error in ZYX-Euler angles (1000 Monte-Carlo runs)


[6] P. Batista, C. Silvestre, and P. Oliveira. Vector-based attitude filter for space navigation. *Journal of Intelligent & Robotic Systems*, 64:221–243, 2011. 10.1007/s10846-010-9528-2.

[7] S. Bhat and D. Bernstein. A topological obstruction to continuous global stabilization of rotational motion and the unwinding phenomenon. *Systems & Control Letters*, 39(1):63–70, 2000.

[8] A.D. Bowen, D.R. Yoerger, C. Taylor, R. McCabe, J. Howland, D. Gomez-Ibanez, J.C. Kinsey, M. Heintz, G. McDonald, D. Peters, et al. The nereus hybrid underwater robotic vehicle. *Underwater Technology: The International Journal of the Society for Underwater*, 28(3):79–89, 2009.

[9] R. W. Brockett. *Finite Dimensional Linear Systems*. Wiley, 1970.

[10] N. Chaturvedi, A. Sanyal, and N. McClamroch. Rigid-Body Attitude Control. *IEEE Control Systems Magazine*, 31(3):30–51, June 2011.

[11] J.L. Crassidis, F.L. Markley, and Y. Cheng. Survey of nonlinear attitude estimation methods. *Journal of Guidance Control and Dynamics*, 30(1):12, 2007.

[12] G. De Novi, C. Melchiorri, J. Garcia, P. Sanz, P. Ridao, and G. Oliver. A New Approach for a Reconfigurable Autonomous Underwater Vehicle for Intervention. In *Proceedings of the 3rd Annual IEEE International Systems Conference*, pages 23–26, Vancouver, Canada, March 2009.

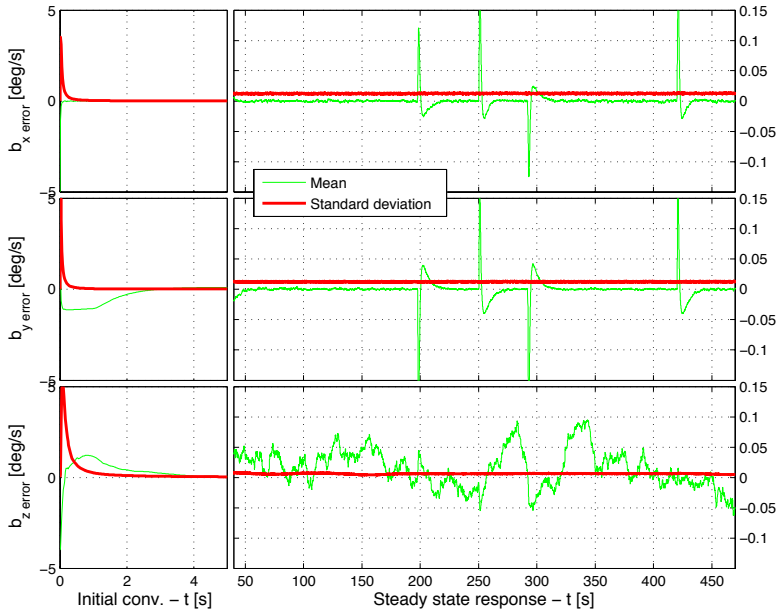


Figure 10: Rate gyro biases estimation errors (1000 Monte-Carlo runs)

[13] A. Gelb. *Applied Optimal Estimation*. MIT Press, 1974.

[14] K. Hayato and T. Ura. Navigation of an AUV for investigation of underwater structures. *Control Engineering Practice*, 12(12):1551 – 1559, 2004.

[15] M. Ignagni. Optimal strapdown attitude integration algorithms. *Journal of Guidance, Control, and Dynamics*, 13:363–369, 1990.

[16] G. Ioannidis. Identification of a Ship or Submarine from its Magnetic Signature. *Aerospace and Electronic Systems, IEEE Transactions on*, AES-13(3):327 –329, May 1977.

[17] J.C. Kinsey, R.M. Eustice, and L.L. Whitcomb. A survey of underwater vehicle navigation: Recent advances and new challenges. In *Proceedings of the 7th Conference on Manoeuvring and Control of Marine Craft (MCMC2006)*, Lisbon, Portugal, 2006. IFAC.

[18] S. Kumar, D.C. Skvoretz, C.R. Moeller, M.J. Ebbert, A.R. Perry, R.K. Ostrom, A. Tzouris, S.L. Bennett, and P.A. Czipott. Real-Time Tracking Gradiometer for use in an autonomous underwater vehicle for buried minehunting. In *Proceedings of the MTS/IEEE OCEANS 2005*, pages 2108 – 2111 Vol. 3, September 2005.

[19] P.M. Lee, B.H. Jeon, S.M. Kim, H.T. Choi, C.M. Lee, T. Aoki, and T. Hyakudome. An integrated navigation system for autonomous underwater vehicles with two range sonars, inertial sensors and Doppler velocity log. In *Proceedings of the*

*MTS/IEEE TECHNO-OCEAN OCEANS'04 Conference*, volume 3, pages 1586–1593, Kobe, Japan, November 2004.

[20] R. Mahony, T. Hamel, and J. Pflimlin. Nonlinear Complementary Filters on the Special Orthogonal Group. *Automatic Control, IEEE Transactions on*, 53(5):1203–1218, 2008.

[21] F.L. Markley. Attitude determination using vector observations and the singular value decomposition. *Journal of the Astronautical Sciences*, 36(3):245–258, 1988.

[22] FL Markley. Optimal Attitude Matrix from Two Vector Measurements. *Journal of Guidance Control and Dynamics*, 31(3):765, 2008.

[23] M. Morgado, P. Oliveira, and C. Silvestre. Design and experimental evaluation of an integrated USBL/INS system for AUVs. In *Proceedings of the 2010 IEEE International Conference on Robotics and Automation ICRA 2010*, pages 4264 –4269, Anchorage, AK, USA, May 2010.

[24] Y.H. Pei, H.G. Yeo, X.Y. Kang, S.L. Pua, and J. Tan. Magnetic gradiometer on an AUV for buried object detection. In *Proceedings of the MTS/IEEE OCEANS 2010*, September 2010.

[25] P. Sanz, P. Ridao, G. Oliver, C. Melchiorri, G. Casalino, C. Silvestre, Y. Petillot, and A. Turetta. TRIDENT: A Framework for Autonomous Underwater Intervention Missions with Dexterous Manipulation Capabilities. In *Proceedings of the 7th Symposium on Intelligent Autonomous Vehicles IAV-2010*. IFAC, 2010.

[26] S. Sastry and C. Desoer. The robustness of controllability and observability of linear time-varying systems. *Automatic Control, IEEE Transactions on*, 27(4):933–939, 2002.

[27] P.G. Savage. *Strapdown Analytics*, volume 1. Strapdown Associates, Inc., Maple Plain, MN, 2000.

[28] M. Shuster. A simple Kalman filter and smoother for spacecraft attitude. *Journal of the Astronautical Sciences*, 37:89–106, 1989.

[29] L.N. Trefethen and D. Bau. *Numerical linear algebra*. Society for Industrial Mathematics, 1997.

[30] K. Vickery. Acoustic positioning systems. New concepts - The future. In *Proceedings of the 1998 Workshop on Autonomous Underwater Vehicles, AUV'98*, Cambridge, MA, USA, August 1998.

[31] G. Wahba. Problem 65 1: A least squares estimate of spacecraft attitude. *Siam Review*, 7(3):409, 1965.

[32] M. Wynn and J. Bono. Magnetic sensor operation onboard an AUV: magnetic noise issues and a linear systems approach to mitigation. In *Proceedings of the MTS/IEEE OCEANS 2002*, volume 2, pages 985 – 993, October 2002.